Reductive sorption of vanadium by green rust in seawater

Author

Haase, FJ, Vessey, CJ, Sekine, R, Welsh, D, Hamilton, J, Wang, Y, White, J, Canfield, DE, Lombi, E, Bennett, WW

Published

2023

Journal Title

Geochimica et Cosmochimica Acta

Version

Version of Record (VoR)

DOI

10.1016/j.gca.2023.07.020

Rights statement

Downloaded from

Griffith Research Online

Geochimica et Cosmochimica Acta 361 (2023) 171–182

Contents lists available at ScienceDirect

Geochimica et Cosmochimica Acta

journal homepage: www.elsevier.com/locate/gca

Reductive sorption of vanadium by green rust in seawater

Felicia J. Haase [a,b,*], Colton J. Vessey [c], Ryo Sekine [d], David Welsh [b], Jessica Hamilton [e], Yun Wang [b], Jessica White [b], Donald E. Canfield [f], Enzo Lombi [g], William W. Bennett [a,b,f]

[a] *Coastal and Marine Research Centre, Griffith University, Southport, QLD 4215, Australia*
[b] *School of Environment and Science, Griffith University, Southport, QLD 4215, Australia*
[c] *Department of Earth and Atmospheric Sciences, Faculty of Science, University of Alberta, Edmonton, Alberta T6G 2R3, Canada*
[d] *School of Science, Technology and Engineering, University of the Sunshine Coast, Moreton Bay Campus, Petrie, QLD 4502, Australia*
[e] *Australian Synchrotron (ANSTO), Clayton, VIC 3168, Australia*
[f] *Nordcee, Department of Biology, University of Southern Denmark, 5230 Odense M, Denmark*
[g] *Future Industries Institute, University of South Australia, SA 5095, Australia*

A R T I C L E I N F O

Associate editor: Caroline L. Peacock

Keywords:
Vanadium
Green rust
Lepidocrocite
Marine sediment
Paleoredox tracer

A B S T R A C T

Vanadium (V) is a redox-sensitive trace metal that typically exists in one of three oxidation states (+3, +4 and +5) in natural waters; a feature increasingly used in paleoredox studies of ancient marine sediments. However, our knowledge of V geochemistry in low-oxygen marine environments is still limited, especially regarding interactions of V with reduced iron minerals such as green rust. Carbonate green rusts (GR_{CO3}) are mixed Fe^{II}/Fe^{III}-phases found in some modern ferruginous settings, such as Lake Matano (Indonesia), and were likely abundant in ancient ferruginous marine systems where they may have played an essential role in authigenic V enrichments in sediments. Here, we present an abiotic pathway of V removal from seawater *via* reduction and adsorption onto amorphous GR_{CO3}. Suspensions of the freshly precipitated GR_{CO3} (1 g L^{-1}) were added to vanadate (1 mg V^{V} L^{-1} initial concentration) in anoxic synthetic seawater solutions. Vanadium removal by GR_{CO3} was rapid and efficient, with 92 – 99% of V removed in under 20 seconds. Synchrotron-based X-ray absorption near edge structure (XANES) spectroscopy showed that V^{V} adsorbed by GR_{CO3} was partially reduced to a mixture of V^{V} and V^{IV}, with the average oxidation state of adsorbed V increasing (+4.3 to +4.7) with increasing solution pH (7.5 to 8.5). Upon subsequent exposure to aerated seawater, V-bearing GR_{CO3} oxidized to lepidocrocite [γ–FeO(OH)] within 24 h, with concomitant reduction of all solid-phase V^{V} to V^{IV}. During oxidation, V was not released back into solution; rather, extended X-ray absorption fine structure (EXAFS) modeling revealed that V^{IV} was structurally incorporated into lepidocrocite as octahedral vanadyl (VO^{2+}). Our work further constrains the aqueous geochemistry of V, which has implications for understanding V cycling and removal mechanisms in both modern and ancient marine systems.

1. Introduction

In aquatic systems, the transition metal vanadium (V) is thermodynamically stable in three oxidation states (+3, +4 and +5) (Baes and Mesmer, 1976; Taylor and Van Staden, 1994; Schlesinger et al. 2017). This unique redox-sensitivity of V has led to its increasing use as a redox proxy to study both modern (e.g., Wang et al., 2019; Bennett and Canfield, 2020) and ancient (e.g., Brumsack 2006; Scholz 2018) sedimentary environments. For example, V was used in a recent interpretation of Mesoproterozoic black shales from the Xiamaling Formation (North China Block), which, combined with other geochemical evidence, suggested that deposition had occurred in oxygenated waters below the anoxic core of an oxygen minimum zone (OMZ); this work had implication for levels of atmospheric oxygen at the time of deposition (Zhang et al., 2016). However, the early diagenesis of V in modern marine sediments is still poorly understood (Ho et al., 2018; Scholz, 2018), particularly in terms of V sorption to particulates in reducing environments (Huang et al., 2015; Gustafsson, 2019; Shaheen et al., 2019).

The fate of V in aqueous environments is dependent on many factors, including: V concentration and speciation, pH, E_h, adsorption/desorption, biological activity, and interaction with major biogeochemical cycles (Baes and Mesmer, 1976; Wanty and Goldhaber, 1992; Crans

* Corresponding author at: Coastal and Marine Research Centre, Griffith University, Southport, QLD 4215, Australia.
E-mail address: felicia.haase@griffithuni.edu.au (F.J. Haase).

https://doi.org/10.1016/j.gca.2023.07.020
Received 29 January 2023; Accepted 25 July 2023
Available online 9 August 2023

et al., 2010). Vanadium exists as a phosphate-like vanadate oxyanion ($H_nV^VO_4{}^{n-3}_{(aq)}$) in most oxic waters, with varying degrees of protonation depending on local pH (Baes and Mesmer, 1976; Sadiq, 1988). Vanadate can also polymerize into a variety of polynuclear species (V_2 to V_6, V_{10}) at vanadium concentrations greater than 100 μM (Baes and Mesmer, 1976; Cruywagen, 1999); however, concentrations in natural waters do not commonly exceed 20 μM (Wanty and Goldhaber, 1992). Vanadyl anions [$V^{IV}O^{2+}$, $V^{IV}OOH^+$, $V^{IV}O(OH)_3^-$] are thermodynamically stable under moderately reducing conditions, such as in ferruginous marine environments (Wehrli and Stumm, 1988; Chen and Liu, 2017), but have been reported in oxic waters alongside V^V (e.g., Wang and Sañudo Wilhelmy, 2008, 2009). Trivalent V exists only under highly reducing conditions, such as euxinic marine environments, and readily precipitates as a solid hydroxide [$V^{III}(OH)_3$] or substitutes for Fe^{III} and Al^{III} in various minerals (Gehring et al., 1994; Balan et al., 2006). Aqueous V^V and V^{IV} can be effectively adsorbed (Krauskopf, 1956; Lewan, 1984; Shieh and Duedall, 1988; Wehrli and Stumm, 1988; White and Peterson, 1996; Morford et al., 2005; Naeem et al., 2007; Brinza et al., 2008; Larsson et al., 2017a; Wisawapipat and Kretzschmar, 2017; Vessey et al., 2020; Vessey and Lindsay, 2020; Zhu et al., 2020; Abernathy et al., 2021; O'Loughlin et al., 2021; Abernathy et al., 2022) and incorporated (Schwertmann and Pfab, 1994; Kaur et al., 2009; Vessey and Lindsay, 2020) by metal (hydr)oxides and sulfides (e.g., of Al, Fe, Mn, Ti), organic matter, and clays. In the modern ocean, for example, iron oxides derived from hydrothermal vents are thought to control V concentrations (Trefry and Metz, 1989). These solid-phase V sorption processes are major pathways for V to transfer from water column to marine sediments, potentially resulting in authigenic V enrichment (Tribovillard et al., 2006; Bennett and Canfield, 2020). Yet, our ability to interpret enrichment in ancient sediments in the context of the prevailing redox conditions requires a better understanding of the geochemical mechanisms driving V uptake in reducing environments (Algeo and Maynard, 2004; Gustafsson, 2019; Shaheen et al., 2019).

Vanadium enrichment is often observed in iron-rich (ferruginous) sedimentary rock formations, such as some banded iron-formations (BIFs) of the Precambrian (Canfield et al., 2018) and early Cambrian (Han et al., 2018), indicating a possible link between iron and vanadium cycling in these ancient reducing environments (Krauskopf, 1956). Green rusts (GRs) are mixed Fe^{II}/Fe^{III} layered double hydroxide minerals (Bernal et al., 1959; Trolard et al., 2007) that occur in modern ferruginous reducing environments such as lake Matano (Indonesia), where aqueous Fe^{II} is partially oxidized in the oxic water column (Zegeye et al., 2012; Etique et al., 2014). Green rust also forms under reducing conditions in soils and sediments (Hansen et al., 1996; Trolard et al., 1997); for example, through bacterial reduction of Fe^{III}-bearing minerals such as ferrihydrite or lepidocrocite (e.g., Ona-Nguema et al., 2002). Carbonate green rusts (GR_{CO3}), a type of GR with interlayers of carbonate anions (CO_3^{2-}), likely occurred in ancient marine systems (Halevy et al., 2017; Koeksoy et al., 2019; Russell and Ponce, 2020) and thus, may have been involved in the sorption and transport of V in ancient marine environments. In laboratory settings, GR can efficiently reduce and sorb various metal(loid)s, such as antimony (e.g., Mitsunobu et al., 2008), arsenic (e.g., Jönsson and Sherman, 2008; Karimian et al., 2017), selenium (e.g., Myneni et al., 1997) and uranium (e.g., O'Loughlin et al., 2003). The reduction of V^V following adsorption in the presence of Fe^{II}-containing phases in solution has been previously described (White and Peterson, 1996; Vessey and Lindsay, 2020; O'Loughlin et al., 2021). While Vessey and Lindsay (2020) and O'Loughlin et al. (2021) observed reduction of V^V and uptake by GR-like secondary phases, a detailed analysis of adsorption kinetics and the reduction–oxidation mechanisms of V by GR_{CO3} in seawater has not been reported.

Recent reviews (Scholz, 2018; Bennett and Canfield, 2020) highlight that V speciation can be utilized to classify the redox chemistry of modern and ancient marine environments (oxic, OMZs and euxinic basins). In reducing environments, minerals that precipitate prior to diagenesis are often exposed to redox fluctuations. For example, authigenic minerals may form in the anoxic water column and then transit to oxygenated bottom waters, or vice versa (Scholz, 2018). There are a number of studies on the direct sorption of V onto iron (oxyhydr) oxides, such as goethite (Schwertmann and Pfab, 1994; Peacock and Sherman, 2004; Kaur et al., 2009; Zhu et al., 2020) and ferrihydrite (Brinza et al., 2008; Larsson et al., 2017a, 2017b; Vessey et al., 2020; Vessey and Lindsay, 2020) — minerals that may be present at the oxygen/$Fe^{II}_{(aq)}$ interface in ferruginous waters (Koeksoy et al., 2016, 2019). Little is known about the fate of reduced iron minerals, and associated metal(loid)s such as V, and their fate and preservation under fluctuating redox conditions. Simulating the effect of diverse oxygen conditions on V-bearing iron minerals, such as GRs, in marine conditions will enable a broader understanding of V speciation and its coordination in environments relevant to both modern and ancient contexts.

To study the kinetics of vanadate sorption by GR_{CO3} in anoxic seawater conditions and subsequent oxidation, we performed batch experiments at environmentally relevant concentrations (1 mg V L^{-1}, Wanty and Goldhaber, 1992) and circumneutral to slightly alkaline pH values (7.5 to 8.5) typical of marine waters. Vanadium oxidation state and coordination environment were determined for both anoxic and oxic conditions using synchrotron-based X-ray absorption near edge structure (XANES) spectroscopy and extended X-ray absorption fine structure (EXAFS) spectroscopy. Our results improve the understanding of the potential role of GR_{CO3} during authigenic enrichment of V within anoxic sediments, and the mobility of V associated with reduced iron minerals under fluctuating redox conditions.

2. Materials and methods

2.1. Reagents and materials

All experimental solutions were prepared with deionized ultrapure (> 18.2 MΩ.cm) (DI) water, which was N_2-purged for a minimum of 2 h and additionally stirred inside an anaerobic chamber (O_2 < 15 ppm, H_2 < 5%; Coy Labs) for at least 10 min to ensure complete degassing. Artificial seawater (ASW) was prepared from a standard laboratory-grade sea salt mix (ASTM D1141-98; Lake Products Company LLC) by dissolving ~42 g of salt per liter of water. Upon dissolution of the salts, the ASW was filtered (Ø 0.2 μm polyethersulfone (PES)) to remove any insoluble components of the salt mix and the pH was adjusted to 8.2 using 0.1 mol L^{-1} HCl. The final salinity of the ASW was 35‰. All chemicals and materials were stored inside the anaerobic chamber for at least one day prior to experiments to minimise the possibility of oxidation by residual O_2 on surfaces. Temperature (SevenCompact™ pH/Ion Meter S220) and pH (SevenCompact™ pH/Ion Meter S220) in solutions were continuously measured, and salinity (Seven2Go Conductivity Meter S3) and DO (Dissolved Oxygen Meter; Mettler Toledo®) were regularly monitored during sorption and oxidation experiments.

2.2. Green rust synthesis and oxidation

Carbonate green rust is the most stable GR-phase in nature (Mills et al., 2012) and was synthesized with the approximate chemical formula $[Fe^{II}_2Fe^{III}_4(OH)_{12}]^{2+}\cdot[CO_3\cdot nH_2O]^{2-}$ ($n \leq 3$) following an adaptation of the co-precipitation method (Drissi et al., 1995), described in detail by Bocher et al. (2004). Quantities of ferrous sulphate heptahydrate ($FeSO_4\cdot 7H_2O$, AR grade) and ferric sulphate hydrate [$Fe_2(SO_4)_3\cdot 4.5H_2O$, LR grade] were each dissolved in 50 mL deoxygenated DI water inside the anaerobic chamber and mixed in a 250 mL glass beaker on a magnetic stirrer, resulting in an approximate initial [Fe^{II}]:[Fe^{III}] ratio of 2.2:1 in solution. In a second step, sodium carbonate (Na_2CO_3 with [CO_3^{2-}] = 0.466 mol L^{-1}, ACS grade) was dissolved in a sodium hydroxide solution ([NaOH] = 0.8 mol L^{-1}, AR grade) and slowly added to the beaker containing the stirred ferrous-ferric iron solution. The formation of sulphate green rust [$GR(SO_4^{2-})$] was avoided by ensuring a ratio of carbonate to sulphate of at least 6:5 (Bocher et al., 2004). The GR_{CO3} precipitate was aged by stirring the solution for 1 h, then recovered by centrifugation at 3000 rcf. The recovered precipitate was washed twice with deoxygenated DI water and once with deoxygenated ASW, being recovered each time by centrifugation at 3000 rcf. The GR_{CO3} dry weight was determined for each experiment by filtering 10 mL of suspension through a Ø 0.03 µm pre-weighed filter, washing the solid with deoxygenated DI water to remove salts, drying it for 24 h inside the anaerobic chamber and reweighing the filter and dried precipitate. Mineral suspensions (1:2 mineral to deoxygenated ASW, or DI water) were prepared to allow accurate addition of green rust to batch reactors. To minimise possible mineral transformations, suspensions were used without delay for sorption experiments and a subsample was taken for X-ray diffraction analysis (XRD; Bruker D4 Endeavour, using Co Kα radiation at 40 kV/40 mA) to confirm the mineral composition at the beginning and end of the experiments. Freshly precipitated GR_{CO3}, as opposed to the freeze-dried form, was used in all experiments to mimic natural conditions of the authigenic formation of (amorphous) green rust in anoxic marine environments. Following the final sampling, subsamples of the final reaction solids were collected by centrifugation for XRD analysis to identify the mineral(s) present. Analogously, a subsample was taken for XRD analysis after exposing the mineral suspension for 24 h to aerated ASW to characterize the oxidation products. A more detailed description of sample preparation for XRD analysis can be found in the Supplementary Material (SM).

2.3. Sorption of V(V) by carbonate green rust

Sorption studies were performed in duplicate to evaluate the kinetics of V adsorption by GR_{CO3} at a pH range relevant to marine environments (pH 7.5, 8.1, 8.5). The reaction solution was made up in 1 L low density polyethylene (LDPE; Nalgene) bottles using ASW at a final salinity of 35 ± 1‰. Freshly synthesized and washed GR_{CO3} was added to batch reactors to achieve a suspension of 1 (± 0.25) g L^{-1} (dry weight). The pH of each kinetics experiment was adjusted after GR_{CO3} addition to 0.1 – 0.2 pH units below the desired final value using 0.2 mol L^{-1} HCl, while stirring the solution vigorously. Vanadate stock solutions ($Na_3V^VO_4$, AR grade; $[V^V]$ = 41.5 mg L^{-1}) were freshly made prior to each experiment to avoid formation of polymeric species. Aliquots of V stock solution were added to batch reactors to yield a final V concentration of roughly 1 (0.9 ± 0.1) mg L^{-1}, resulting in final loadings of around 1000 µg V g^{-1} GR_{CO3} (Table S1). The solution pH was only adjusted at the start of the sorption experiments to desired values and was relatively stable throughout the 4-hour experiment, with a maximum increase of 0.15 units. The temperature inside the batch reactors was controlled using a custom-built water-jacket system and kept at 25.0 (± 0.2) °C. Following the addition of vanadate, subsamples of the solution were collected at 15 time points: 10, 20, 40, 60, 90, 120, 180 s, and 10, 20, 40, 60, 90, 120, 180 and 240 min. Subsamples were collected using 20 mL polypropylene syringes (HSW, Norm-Ject®) and filtered through Ø 0.45 µm and 0.03 µm pore size PES filter membranes mounted in series to separate solid- and solution-phases. Residual V and Fe in filtered aqueous samples were measured directly by inductively coupled plasma mass spectrometry. Solid-phase samples from the kinetics experiments were collected on Ø 0.45 µm pore size filter membranes and dried over 1 to 2 days inside the anaerobic chamber. The dried solid was carefully scraped off the filter membrane, homogenized, spread on to carbon tape (C-tape) and mounted on polymethyl methacrylate sample holders inside the anaerobic chamber. Mounted samples were covered with parafilm to avoid cross-contamination and stored in sealed aluminized Mylar bags under an N_2 atmosphere at –80 °C until further analysis at the Australian Synchrotron.

In a separate set of experiments, adsorption isotherms for the pH values of 7.5, 8.1, and 8.5 were determined using batch reactors (0.25 L Nalgene LDPE bottles) containing varying initial V:GR_{CO3} mass ratios (0 – 300 mg V g^{-1} GR_{CO3}). The pH change of the solution caused by vanadate and GR_{CO3} addition was tested in advance and accounted for. This was done by adjusting the pH after vanadate addition to 0.1 – 0.2 pH units lower than the desired pH in anticipation of an expected pH increase caused by the GR_{CO3} addition (Table S2). The batch reactors were continuously shaken at a constant temperature of 25.0 ± 1.5 °C until equilibrium was reached (t = 2 h), at which point aqueous and solid samples were collected, preserved and analyzed as outlined above. The Microsoft Excel-based user interface (UI) developed by Wang and Guo (2020) was used to fit various models to the adsorption isotherm data of the V–GR_{CO3} system. The empirical, non-linear Freundlich model (Freundlich, 1906) with the adsorbate concentration C_e, the adsorbed amount q_e, and isotherm constants K_F ($L^{1/n} \cdot mg^{1-1/n} \cdot g^{-1}$) and n; and the chemical adsorption model after Langmuir (Langmuir, 1916, 1918) with isotherm adsorption constants K_L (L mg^{-1}) and q_{max} (g mg^{-1}), are typically used to describe adsorption isotherms. For n = 1, the Freundlich model equals the Linear model.

2.4. Oxidation of V-bearing green rust

Following each kinetic sorption experiment, oxidation of V-bearing GR_{CO3} was performed for the three different pH treatments (7.5, 8.1, 8.5; Table S3). After adsorption, batch reactors were removed from the anaerobic chamber and exposed to ambient air for 24 h while constantly and vigorously (~800 – 900 rpm) being stirred on a magnetic stirrer. For the pH 8.5 treatment, samples were collected at 13 time points (30, 60, 120, 240 s and 10, 20, 40, 60, 120, 240, 480, 960 and 1440 min) from the batch experiment. Whereas, for pH 7.5 and 8.1 experiments, samples were collected only at the end of the reoxidation experiment (1440 min). Solution samples were collected, filtered and membrane filters and filtrate were preserved as described above for the sorption experiments. Note here that the membrane filters were directly transferred to the anaerobic chamber to dry and were processed alongside the adsorption samples in an N_2 atmosphere to prevent potential further oxidation.

2.5. Sample analysis

2.5.1. Inductively coupled plasma mass spectrometry

Inductively coupled plasma-mass spectrometry (ICP–MS; Agilent 7900) was used to measure concentrations of residual dissolved V and Fe in experimental solutions. Samples were diluted 10-fold in deionized water and acidified with ultrapure nitric acid to 2% (v/v) prior to analysis. The instrument was run in high-matrix introduction (HMI–4) mode with nebulizer gas flow at 0.75 L min^{-1} and dilution gas flow at 0.3 L min^{-1} to minimize the impact of the seawater matrix on instrument stability. Accuracy of the ICP–MS analysis was verified by analyzing a seawater certified reference material (CASS–5; National Research Council Canada) in each analytical run, and results agreed to within 94 – 109% of the certified value of 1.32 µg V L^{-1} (average measured concentration: 1.38 µg V L^{-1}). The limit of detection (LOD) was calculated as three times the standard deviation of ASW blanks and ranged from 0.0035 to 0.095 µg V L^{-1}.

2.5.2. X-ray absorption spectroscopy

2.5.2.1. Data collection. Synchrotron-based X-ray absorption spectroscopy (XAS) was performed at the XAS beamline of the Australian Synchrotron (Clayton, VIC). The storage ring operated at 3 GeV in top-up mode with a maximum electron current of 200 mA. XAS spectra were collected at the V *K*-edge (5463.76 eV) using a Si[1 1 1] double-crystal monochromator. Note here that the monochromator of the Australian Synchrotron is calibrated to a tabulated value of 5463.76 eV (Kraft et al., 1996), which then was corrected during data processing to the more commonly used value of 5465 eV for the V *K*-edge (for more details see 2.5.2.3). Solid-phase XAS standards and samples on C-tape were measured at room temperature in an He-sparged sample cell. XANES and EXAFS spectra were collected in fluorescence mode with a 100-pixel monolithic HP-Ge fluorescence detector (CANBERRA, France) over the pre-edge region (5400 – 5462 eV) in 3 eV steps and the XANES region (5462 – 5517 eV) in 0.25 eV steps. The EXAFS region was scanned in steps constant in k space (0.035 $Å^{-1}$) up to $k_I = 14$ $Å^{-1}$ for experiments conducted at pH 8.5. Samples collected from experiments at pH 7.5 and 8.1 were scanned up to $k_{II} = 12.5$ $Å^{-1}$. Spectra were collected in triplicate for each sample and a reference vanadium metal (V^0) foil was scanned with each spectrum to calibrate spectra for energy shifts during the beamtime. Sample-alteration due to radiation damage was assessed by our group previously for similar samples (i.e., V-bearing iron monosulfide) by rapidly scanning the same sample spot and monitoring changes in pre-edge peak height and main edge position — damage was negligible for exposure times representative of typical EXAFS scans. Further beamline and scan details for XAS measurement of V are discussed elsewhere (Bennett et al., 2018), and were followed as outlined therein.

2.5.2.2. Vanadium reference standards. Reference materials for V species (V^V, V^{IV} and V^{III}) were prepared using commercial ACS-grade standards (Sigma Aldrich, > 99%), including sodium orthovanadate ($Na_3V^VO_4$), V^V oxide (V_2O_5), vanadyl sulfate pentahydrate ($V^{IV}OSO_4 \cdot 5H_2O$), V^{IV} oxide (VO_2) and V^{III} oxide (V_2O_3), which were collected over multiple beamtime sessions using identical settings of measurement parameters, some of which were previously published by Bennett et al. (2018). In addition, standards of $V^{IV}O(OH)_2$ and $V^{III}(OH)_3$ were freshly prepared at the beamline *via* neutralization of VCl_3 and $VOSO_4$ with sodium hydroxide, until a precipitate formed and were then directly analyzed. An additional V^{III} standard ($V^{III}Cl_3$) from Vessey and Lindsay (2020) was used for the XANES data analysis. Previous dilution of V reference standards with cellulose resulted in significant reduction of V^V during X-ray exposure, therefore, reference materials were used in undiluted form. Powders were spread as a thin layer (to avoid self-absorption) using a fine brush directly onto separate C-tape sections mounted onto XAS holders, which were then covered with parafilm to prevent contamination during storage. For all standards and samples, the parafilm was then removed directly before analysis.

2.5.2.3. Data processing and analysis. Initial data conversion and reduction was done using the pre-processing tool SAKURA (https://www.ansto.gov.au/our-facilities/australian-synchrotron/synchrotron-beamlines/x-ray-absorption-spectroscopy/sakura-a). Alignment of reference channels and calibration to 5465 eV (first peak of the first derivative), energy normalisation, deglitching of spectra, and data reduction was done using ATHENA software (Demeter version 0.9.26; Ravel and Newville, 2005). XANES data was analyzed in OriginPro (2021b) by auto-fitting a linear baseline to the selected energy region (5460 – 5480 eV) and the area integrated between the baseline and the pre-edge peak (PEP). Linear baselines were manually adjusted where needed to optimize fits. The mathematical area of vanadium PEP features was determined for relevant vanadium standards and based on the linear relationship of PEP area versus average oxidation state of standards, the oxidation states of samples were mathematically calculated within the 95% confidence interval (CI). EXAFS data was analyzed using ARTEMIS (Demeter, version 0.9.26; Ravel and Newville, 2005), the absolute zero of energy (E_0) was chosen as the first peak in the first derivative of each spectrum. Experimental Fourier-transformed χ(R) data was fitted using theoretical scattering paths from modified FEFF calculations of V standards ($Na_3V^VO_4$, $V^{IV}OSO_4$) and mineral structures (i.e., lepidocrocite) for substitution of structural Fe^{III} by V. Based on knowledge of common vanadium coordination environments, theoretical single and multiple scattering paths of standards were compared to experimental EXAFS oscillations for varying k-ranges to obtain initial fits. Nonlinear least-squares fitting of EXAFS data was done progressing shell-by-shell to account for all characteristic features of the pseudo-radial distribution function for each sample. Further optimisation of fits was done by refinement of the Debye-Waller factor (σ^2), coordination number (N), V–X distance (R) and energy shift (ΔE_0). The amplitude reduction factor (S_0^2) was fixed at a value of 0.90 as an approximation, resulting in good fits for standards and samples. Statistical significance was assessed using the Hamilton test (Calvin, 2013).

3. Results

3.1. Mineral identities

Comparison of XRD spectra with those on the International Centre for Diffraction Data (ICDD) database resulted in a match of the synthesized mineral with trébeurdenite ($Fe_2^{II}Fe_4^{III}O_2(OH)_{10}CO_3 \cdot 3H_2O$; Génin et al., 2014), which is referred to hereafter as GR_{CO3}. The (amorphous) GR_{CO3} was the only phase before and after sorption of V. XRD analysis of the oxidation product showed that GR_{CO3} fully transformed to lepidocrocite [γ-FeO(OH)] within 24 h of exposure to oxic conditions.

3.2. Reductive sorption of V(V) by green rust

3.2.1. Kinetics

Green rust sorbed 92 to 99% of aqueous vanadate ($H_nV^VO_4^{n-3}$) within 20 seconds of GR_{CO3} addition (Fig. 1). Equilibrium (defined here as a concentration change of ≤ 0.50%) was reached within 120 s, with

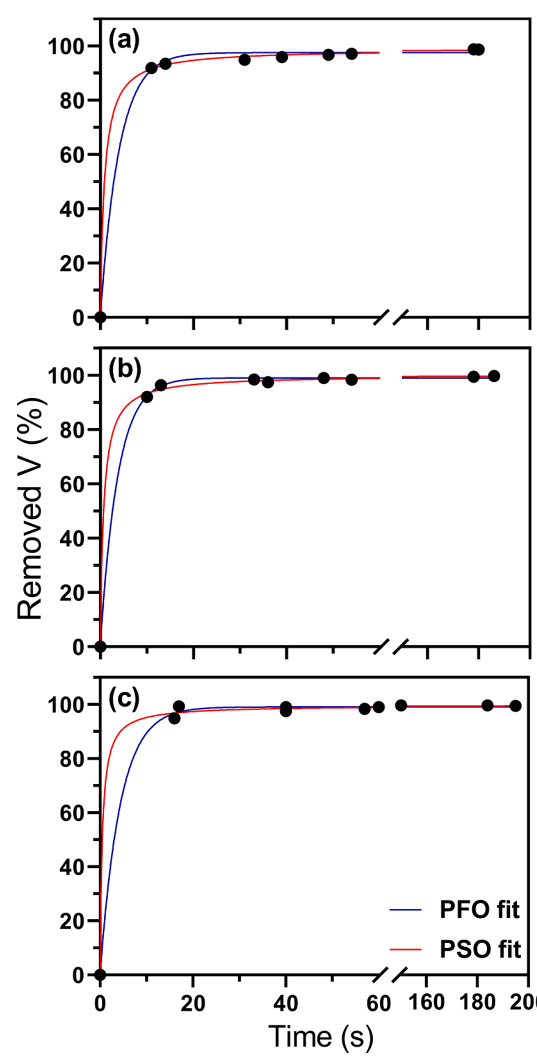

Fig. 1. Percentage of vanadate removal by green rust (1000 μg g^{-1}) at: (a) pH 7.5, (b) pH 8.1 and (c) pH 8.5. The blue line indicates pseudo-first order (PFO) and the red line corresponds to pseudo-second order (PSO) kinetic fits.

more than 98% of V (1 mg L^{-1}) removed from solution. The pH had, as anticipated, an effect on the solubility of GR_{CO3} in solution, resulting in decreased GR_{CO3} dissolution and lower Fe^{II} concentrations in solution at higher pH values (Table S4). However, rapid sorption of V by GR_{CO3} was consistent for all tested pH values regardless of solubility-related differences in V-mineral loadings (0.7 – 1.3 mg V g^{-1} GR_{CO3}; $Fe^{II}_{(aq)}$: 0.14 – 1.4 mM). Due to the almost instantaneous sorption of nearly all V (≥ 92%) in solution, attempts to capture the initial linear section of the sorption process were not successful. As a result, both pseudo-first and pseudo-second order model fits described the sorption equally well, with $R^2 > 0.998$ for all fits of both models (Table S5). Previously, a multiple reaction pathway model for vanadate sorption has been introduced (Vessey and Lindsay, 2020), which as a consequence of the instantaneous nature of the V–GR_{CO3} reaction could not be applied here. Even when reducing the reaction temperature to 5 °C, the majority of V (> 83%) was removed within the first feasible sampling time point (~15 s), and more than 93% within the first 120 s (Fig. S1).

3.2.2. Adsorption isotherms

Adsorption isotherm data was fit to the Freundlich (K_F, log K_F and n), Langmuir (K_L and q_{max}) and Linear model (K) (Table 1 and Fig. 2; Wang and Guo, 2020). Lower V concentrations have a higher relevance to marine settings, therefore, we selected the fitting range up to 6 mg V g^{-1} GR_{CO3} mass ratio (< 300 ppb $[V]_{initial}$) in solution for non-linear Freundlich and Langmuir fits and fitted a reduced range of both 1.5 and 0.6 mg V g^{-1} as the upper limit of linearity for linear fits. The Langmuir model fit resulted in high R^2 values in the range of 0.997 to 0.999, although the Freundlich model provided a slightly better fit for pH 7.5 ($R^2_F = 0.9992$ versus $R^2_{LA} = 0.9972$) with K_F ranging from 10.7 to 97.4 mg V g^{-1} GR for pH 7.5 to 8.5. The Linear model of the isotherm was done selectively for the linear section of the initial sorption and fits were overall slightly better for the range '0 – 0.6 mg V g^{-1}' compared to the range up to 1.5 mg V g^{-1}, with R^2_L in the range of 0.9702 to 0.9964 and K ranging from 52.5 to 99.6. Overall based on coefficient of determination (R^2) values, both the Langmuir and the Freundlich model provided good fits for the data. Generally, we observed that V^V adsorption onto GR_{CO3} increased with increasing pH from 7.5 to 8.5. Alternative isotherm fits using Scatchard plots (Scatchard, 1949; Abernathy et al., 2022) were done (Fig. S2). However, the single-site Langmuir model and the Freundlich model described the data better ($R^2 > 0.99$) than linear conversions of Scatchard plots ($R^2 < 0.87$).

3.3. Oxidation of V-bearing green rust

We observed complete oxidation of the dark green-blue GR_{CO3} to the bright orange colored lepidocrocite (LP) during 24 h of aeration with ambient air, coupled with a substantial pH decrease (pH 8.43 to 7.99; pH 8.17 to 7.75; pH 7.59 to 4.87; Table S3). Only minor amounts of adsorbed V (< 4 μg L^{-1}, or < 0.5%; Table S6) were released after 20 to 40 min following oxidation (pH 8.5), which were then fully re-adsorbed onto the newly formed LP at the next sampling time point and remained associated with the solid-phase for the duration of the experiment (Fig. S3).

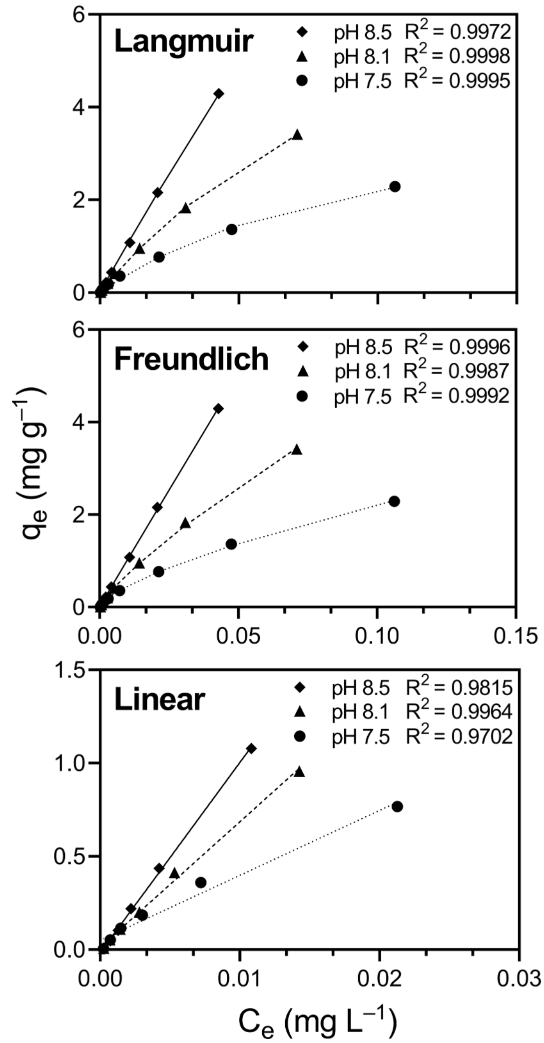

Fig. 2. Adsorption isotherms with Langmuir, Freundlich and Linear model fits for removal of V by GR_{CO3} in anoxic marine waters, where C_e and q_e are the adsorbate concentration (mg L^{-1}) and adsorbed amount (mg g^{-1}), respectively. Langmuir and Freundlich fit ranges were up to 6 mg g^{-1} V:GR_{CO3} mass ratio in solution and up to 0.6 mg g^{-1} V:GR_{CO3} for Linear fits.

3.4. Vanadium K-edge XANES and EXAFS

Vanadium *K*-edge XANES spectra of reference materials and samples were evaluated to obtain information on valence states and symmetries of sorbed V associated with GR_{CO3} and LP (Wong et al., 1984; Haskel et al., 2004; Chaurand et al., 2007; Levina et al., 2014; Duchesne et al., 2016; O'Loughlin et al., 2021). Linear combination fitting (LCF) in Athena was attempted but was not successful due to different V symmetries of samples compared to measured standards. Therefore, quantitative analysis using the PEP method (e.g., Chaurand et al., 2007;

Table 1
Summary of V–GR_{CO3} adsorption isotherm parameters generated using the UI by Wang and Guo (2020), including K_F ($L^{1/n} \cdot mg^{1-1/n} \cdot g^{-1}$), log K_F and n obtained from Freundlich, K_L (L mg^{-1}) and q_{max} (mg g^{-1}) obtained from Langmuir and K (L g^{-1}) obtained from Linear model fits.

	Langmuir model			Freundlich model				Linear model			
Fitting range	**0 – 6** mg V g^{-1}			**0 – 6** mg V g^{-1}				**0 – 0.6** mg V g^{-1}		**0 – 1.5** mg V g^{-1}	
pH	K_L	q_{max}	R^2	K_F	log K_F	n	R^2	K	R^2	K	R^2
7.5	9.81	4.45	0.9972	10.7	1.03	1.46	0.9992	52.5	0.9702	38.1	0.9639
8.1	7.57	9.76	0.9998	28.8	1.46	1.25	0.9987	76.2	0.9964	68.5	0.9953
8.5	1.71	62.8	0.9995	97.4	1.99	1.01	0.9996	99.6	0.9815	99.7	0.9976

Levina et al. 2014; Benzi et al., 2016) was done by comparison of the PEP intensities of samples to those of selected V reference spectra using a linear regression ($R^2 = 0.997$). An average valence state of +5.1 ± 0.1 for $Na_3V^VO_4$ and an average +3.9 ± 0.2 for $V^{IV}OSO_4$ were calculated within the 95% confidence interval (Table S7). Analysis of samples using the PEP method revealed that adsorption of V^V onto GR_{CO3} resulted in partial reduction, yielding mixtures of V^V and V^{IV} species, with average oxidation states of +4.3 (pH = 7.5), +4.4 (pH = 8.1) and +4.7 (pH = 8.5). As pH increased throughout the adsorption experiments, V had a higher average oxidation state. Interestingly, after exposing the reaction solution for 24 h to aerated seawater, average V oxidation states decreased further to +4.0 (pH = 7.5), +3.9 (pH = 8.1) and +3.9 (pH = 8.5) during the transformation of GR_{CO3} to LP (see Fig. 3). Additionally, a significant pH decrease (down to as low as pH 5) was observed during the formation of the (oxyhydr)oxide mineral LP.

Collected EXAFS spectra of reference materials and samples were analyzed using nonlinear least-squares fitting to obtain information on the coordination environments of V–GR_{CO3} and V–LP complexes, which ultimately gives information on sorption processes and stability of products (Fig. 4; Table 2). The $Na_3V^VO_4$ standard was fit as previously reported (Brinza et al., 2019; Larsson et al., 2017a; Vessey and Lindsay, 2020) to a first shell V^VO_4 tetrahedron at 1.72 Å and a second shell multiple scattering path (V—O—O) with a coordination number of 12 at 3.12 Å. The $V^{IV}OSO_4$ standard exhibited a distorted VO_6 octahedron as previously reported (Cooper et al., 2003; Krakowiak et al., 2012; Wen et al., 2016; Vessey and Lindsay, 2020), with a characteristic short first shell V═O double bond at ~1.59 Å, four equatorial V—O bonds at around 2.01 Å, a *trans* V—O bond at an interatomic distance of 2.53 Å and a fourth shell V—S backscatter path at 3.28 Å. Coordination numbers (CNs) for the first shell in V–GR_{CO3} complexes were in a first approximation calculated based on the interpretation of V^V/V^{IV} ratios in samples derived from quantitative XANES analysis (see EQ. S1 and S2). Due to a slight mismatch of fit and data, a second approach was taken where CNs were permitted to float. This resulted in elongated first shell V—O interatomic distances for V–GR_{CO3} fits of ~1.68 Å and CNs between 2 and 3, potentially representing a mixture of octahedrally coordinated V^{IV} (1 coordinate V═O ligand at ~1.59 Å) and tetrahedrally coordinated V^V (4 V—O ligands at ~1.72 Å). Second shell V—O bonds were fit to interatomic distances of ~1.99 Å, and CNs were between 2 and 4 for all V–GR_{CO3} experiments. Two coordinate V···Fe backscatters at ~3.35 Å indicate a bidentate corner-sharing complexes with GR_{CO3}. At pH 7.5 and pH 8.1, one coordinate V···Fe around 3.37 and 3.34 Å were present. Long-range V···Fe backscatters were also present in solids collected from reactions at pH 7.5 (3.84 Å), pH 8.1 (3.91 Å) and 8.5 (4.02 Å), which are indicative of monodentate bonds. However, this bond distance is slightly longer than previously reported monodentate V···Fe distances (~3.6 Å) for vanadate adsorption onto siderite (Vessey and Lindsay, 2020). Statistical analysis of backscatter paths using the Hamilton test showed that the addition of the V···Fe path at ~3.35 Å (p = 0.045) for experiments with GR_{CO3} at pH 8.5 resulted in statistically significant improvements to the fit (Table S9). However, the addition of V···Fe paths (p > 0.05) for experiments with GR_{CO3} at pH 7.5 and 8.1 did not significantly improve the fit. This statistical uncertainty could originate from a low signal-noise ratio during data collection in EXAFS region and may be minimized by extending the scan past 14 $Å^{-1}$ for future experiments.

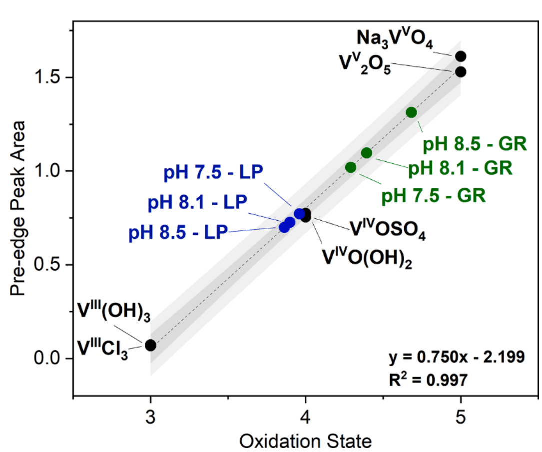

Fig. 3. Linear regression of pre-edge peak area versus oxidation state of vanadium reference standards (black) with the 95% confidence band (dark grey) and the 95% prediction band (light grey). Calculated V oxidation states of V-bearing green rust (GR) samples are plotted in green and those of oxidized V-bearing GR, lepidocrocite (LP) samples, in blue.

EXAFS modeling of V–LP samples at all three pH treatments revealed not only a change in associated V oxidation states, but also a change of V coordination environments upon oxidation. Lepidocrocite has an orthorhombic crystal structure (Ewing, 1935) with a distorted Fe—O octahedron. Oxidized samples were fit by replacing a structural Fe atom in LP with a V atom in the CIF file used to model the samples. Vanadium incorporated into LP exhibited an octahedral coordination for pH 7.5, with one V—O bond around ~1.65 Å, a 4 coordinate equatorial V—O path at ~2.00 Å, and one V—O bond at ~2.38 Å. We are uncertain if the V═O double bond is retained here or if the vanadyl octahedron is simply distorted. For pH 8.1 and 8.5, fit results were improved by fitting two V—O bonds at ~1.70 Å and a 4 coordinate equatorial V—O path at ~1.99 Å. Together, with a large V···Fe backscatter path at ~3.0 Å in 6 coordination, the results indicate that V^{IV} replaced octahedral Fe^{3+} and, therefore, was incorporated into the structure of the newly formed LP. Structural incorporation of V^{IV} can visually be seen in the pronounced V···Fe backscatter feature (Fig. 4) and could also explain the stability of the reduced V species even when exposed to oxic conditions for 24 h.

4. Discussion

4.1. Green rust characterization

The current ICDD database does not differentiate between the two carbonate green rust mineral phases fougèrite ($Fe^{II}_4Fe^{III}_2(OH)_{12}CO_3 \cdot 3H_2O$), which has a ferric molar ratio of x = 0.33, and trébeurdenite ($Fe^{II}_2Fe^{III}_4O_2(OH)_{10}CO_3 \cdot 3H_2O$), which has a ferric molar ratio of x = 0.67. However, Mills et al., 2012 have clearly reclassified GR-like phases using spectroscopic characteristics. Additional manual comparison and calculations of d-spacing using the software Match! (Version 3.13, Crystal Impact, Germany) and comparison of the (0 0 3) and (0 1 2) peak positions to other literature (Génin et al., 2014; Ruby et al., 2010) confirmed the presence of trébeurdenite. Direct quantitation of $Fe^{II}_{(aq)}$ and total Fe following dissolution in concentrated HCl (after Kostka and Luther III, 1994) gave ferric molar ratios of x = 0.41 (after synthesis) and x = 0.44 (after V sorption). This suggests that the synthesized mineral had a composition that was either a mix of or an intermediate form between the two previously described carbonate green rust minerals, fougèrite and trébeurdenite, and is referred to as GR_{CO3} herein.

4.2. Kinetics

Green rust showed a high affinity to fully sorb environmentally relevant amounts of V (1000 μg or ~20 μmol V g^{-1} GR_{CO3}; Huang et al., 2015; Wanty and Goldhaber, 1992) within the pH range of natural seawater (pH 7.5 – 8.5). The sorption was remarkably rapid and in comparison to other pseudo-first and pseudo-second order k values found in the literature, our values (k_1 0.13 – 0.27 s^{-1} and k_2 of 0.91 – 3.5 g mg^{-1} s^{-1}) were within the upper range of reported kinetic values for comparable metal(loid) removal by GR_{CO3} or other iron minerals (Table 3). Adsorption kinetics are influenced by the adsorbent:adsorbate ratio, which in this kinetic study was in the lower range (0.1% V loading) compared to other studies (Williams and Scherer, 2001; Bond and Fendorf, 2003; Perez et al., 2019; Vessey and Lindsay, 2020; Zhu

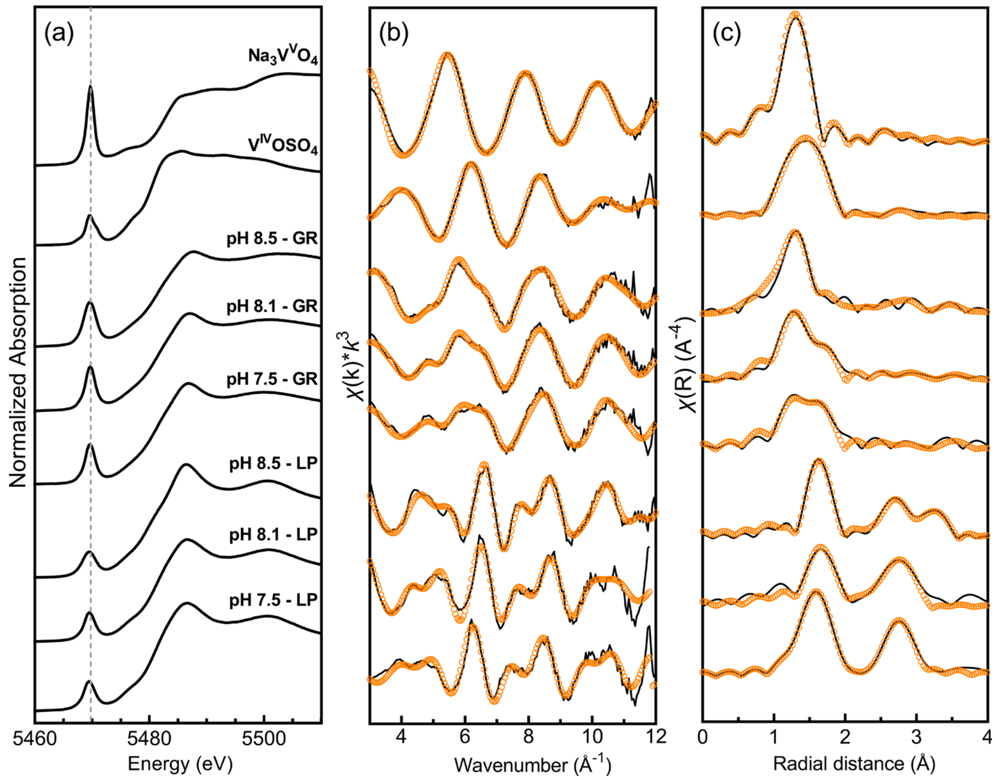

Fig. 4. Vanadium *K*-edge XANES and EXAFS regions for V reference standards ($Na_3V^VO_4$, $V^{IV}OSO_4$), V adsorbed onto green rust (GR) at pH 7.5, 8.1 and 8.5 in anoxic seawater, and V structurally incorporated into lepidocrocite (LP) following oxidation in aerated seawater. Black lines show collected spectra, while empty orange circles correspond to EXAFS fits.

Table 2
Summary of EXAFS parameters for V reference standards and sorption/oxidation samples. Parameters include the amplitude function (S_0^2), the energy-shift (ΔE), the coordination number (CN, *restrained), bond distance (R), the Debye-Waller factor (σ^2), and reduced chi-squared (X^2_{red}).

Sample ID	k-range	S_0^2	ΔE	X^2_{red}	R factor	Paths	CN	R (Å)	σ^2 (Å^2)
$Na_3V^VO_4$	3 – 12	0.9	−4.4(4)	64.8	0.019	*V–O*	4.0*	1.715(4)	0.0042(2)
						V–O–O MS	12.0*	3.12(3)	0.004(4)
$V^{IV}OSO_4$	3 – 12	0.9	8.6(6)	131	0.014	*V–O1*	1.0*	1.597(6)	0.0007(6)
						V–O2	4.0*	2.014(9)	0.0055(5)
						V–O3	1.0*	2.53(5)	0.012(7)
						V–S	2.0*	3.28(4)	0.018(6)
V–GR pH 8.5	3 – 14	0.9	4.8(5)	7.68	0.020	*V–O1*	2.64(9)	1.678(4)	0.0079(1)
						V–O2	3.7(3)	1.989(5)	0.0062(9)
						V–Fe1	2.0(5)	3.35(2)	0.018(4)
						V–Fe2	0.8(4)	3.84(3)	0.011(6)
V–GR pH 8.1	3 – 12	0.9	1(1)	28.3	0.028	*V–O1*	2.3(1)	1.68(5)	0.0048(4)
						V–O2	2.2(2)	1.98(6)	0.0051(7)
						V–Fe1	0.96(4)	3.34(4)	0.014(4)
						V–Fe2	2.0(9)	3.91(5)	0.018(7)
V–GR pH 7.5	3 – 12	0.9	2.5(9)	66.9	0.070	*V–O1*	2.06(3)	1.68(2)	0.005(1)
						V–O2	3.19(4)	1.98(2)	0.007(1)
						V–Fe1	0.5(6)	3.31(9)	0.01(1)
						V–Fe2	0.5(3)	3.85(5)	0.006(6)
V–LP pH 8.5	3 – 14	0.9	5.6(5)	44.0	0.029	*V–O1*	2.0*	1.70(1)	0.008(2)
						V–O2	4.0*	1.99(1)	0.0053(6)
						V–Fe1	6.0*	3.01(1)	0.018(1)
						MS	2.0*	3.73(1)	0.003(1)
						V–O3	4.0*	3.93(2)	0.005(3)
V–LP pH 8.1	3 – 12	0.9	8.1(5)	93.1	0.028	*V–O1*	2.0*	1.71(1)	0.009(2)
						V–O2	4.0*	1.997(8)	0.0071(9)
						V–Fe1	6.0*	3.053(8)	0.014(1)
						MS	6.0*	3.30(3)	0.003(4)
V–LP pH 7.5	3 – 12	0.9	9.2(7)	64.7	0.038	*V–O1*	1.0*	1.658(5)	0.0013(7)
						V–O2	4.0*	2.003(4)	0.0064(5)
						V–O3	1.0*	2.38(2)	0.009(3)
						V–Fe	6.0*	3.08(1)	0.014(1)

Table 3
Kinetic parameters k_1 (in s^{-1}) for pseudo-first order and k_2 ($g\ mg^{-1}\ s^{-1}$) for pseudo-second order nonlinear fits of V–GR_{CO3} system (this paper) in comparison with reported k values of diverse studies of either GR kinetics with comparable metal(loid)s (As, Cr) or V^V with other iron minerals.

Reference	Adsorbent	Adsorbate	Pseudo first-order k_1 (s^{-1})	Pseudo second-order k_2 ($g\ mg^{-1}\ s^{-1}$)
Bond and Fendorf, 2003	Green rusts [0.125 – 0.5 g L^{-1}]	Cr(VI) [25 – 125 μM]	GR_{Cl}: 1.3×10^{-3} – 3.7×10^{-2} GR_{CO3}: 1.9×10^{-3} – 2.4×10^{-2} GR_{SO4}: 6.1×10^{-4} – 1.8×10^{-2}	—
Perez et al., 2019	Sulfate green rust [4 g L^{-1}]	As(III;V) [133 μM]	—	As(III): 0.11As(V): 0.36
This study	**Carbonate green rust** [1 g L^{-1}]	**V(V)** [20 μM]	**0.13 – 0.27**	**0.91 – 3.5**
Vessey and Lindsay, 2020	Ferrihydrite	V(V) [100 μM]	3.3×10^{-3}	—
	Magnetite		2.5×10^{-2}	—
	Siderite		—	3.2×10^{-2}
	Mackinawite [all 2 g L^{-1}]		3.8×10^{-2}	—
Williams and Scherer, 2001	Carbonate green rust [0.25 g L^{-1}]	Cr(VI) [100 μM]	3.0×10^{-3} – 4.4×10^{-3}	—
Zhao et al., 2021	Chloride green rust [~0.45 g L^{-1}]	Cr(VI) [10 mM]	1.4×10^{-2}	—
Zhu et al., 2020	Goethite [2 g L^{-1}]	V(V) [~5 mM]	6.7×10^{-5}	6.2×10^{-4}
	Birnessite [2 g L^{-1}]		1.0×10^{-4}	2.7×10^{-4}

et al., 2020; Zhao et al., 2021). A general excess of available GR_{CO3} adsorption sites (due to low V concentrations) can therefore be assumed in our study. The sorption capacity of fougèrite for As^V, for example, was reported to be > 3300 μmol g^{-1} (Jönsson and Sherman, 2008), which is 165 times higher than the loading of this study. However, compared to modern marine contexts (average of 1.63 – 2.5 μg V L^{-1} (ppb); Collier, 1984; Jeandel et al., 1987), the concentrations used, both for V and GR, can still be considered high. For ancient marine contexts, deposition of higher V concentrations over geologic time scales are assumed (90 ppm; Goldschmidt, 1937; Krauskopf, 1956) and black shales often contain high V concentrations up to several 1000 ppm (e.g., Vine and Tourtelot, 1970; Bian et al., 2022).

4.3. Adsorption isotherms

The adsorption capacity of GR_{CO3} for V, based on K_F from the Freundlich model and q_{max} from Langmuir model, is within the higher range of previously reported values, especially for pH values 8.1 and 8.5 (Naeem et al., 2007; Prathap and Namasivayam, 2010; Kong et al., 2020; Vessey et al., 2020; Zhu et al., 2020; Gonzalez-Rodriguez and Fernandez-Marcos, 2021; Table 4). The pH 8.5 isotherm fit constant (K_F), for example, is almost double that for commercially available metal hydroxide adsorbents used by Naeem et al. (2007), which indicates a high V adsorption capacity of GR_{CO3} in seawater.

Generally, we observed that vanadate adsorption onto GR_{CO3} increased with increasing pH from 7.5 to 8.5. Other studies observed the opposite trend for the adsorption onto other metal (oxyhydr)oxides, with vanadate forming a pH-dependent adsorption envelope (pH 4 – 9) through ligand exchange and competition with OH^- ions at higher pH values (Peacock and Sherman, 2004; Naeem et al., 2007; Prathap and Namasivayam, 2010). The dissolution of GR_{CO3} at the lower pH values could be a possible explanation for the observed trends. Carbonate green rust is also known to grow by Ostwald-ripening — a sequence of dissolution and (co-)reprecipitation — which can obscure pH-dependence for the adsorption of ions (Guilbaud et al., 2013). We did not observe any release of V to solution during adsorption, which provides evidence that the bulk of V remained adsorbed even if GR_{CO3} underwent Ostwald-ripening or dissolution during the study. Comparing our results to similar studies, some other factors such as the partial reduction of V^V to V^{IV} by GR_{CO3} and the higher ionic strength used (seawater = 35‰) should be considered. The higher ionic strength can generally enhance aggregation of particles and therefore, reduce sorption sites (Shieh and Duedall, 1988). The point of zero charge (PZC) of freshly precipitated GR_{CO3} was previously determined to be approximately at pH 8.35 ± 0.05 (Guilbaud et al., 2013); consequently, GR_{CO3} has a positive surface charge for pH smaller than 8.35 favoring the adsorption of anionic vanadate ($H_2V^VO_4^-$ and $HV^VO_4^{2-}$), and a negative charge for pH greater than 8.35, which is less favorable for vanadate adsorption. There are, however, also reports of HVO_4^2– specifically and fully binding to negative oxide surfaces up to pH 8.5 (Wehrli and

Table 4
Examples of Freundlich (K_F in $L^{1/n} \cdot mg^{1-1/n} \cdot g^{-1}$ and n) and Langmuir (q_{max} in mg g^{-1} and K_L in L mg^{-1}) parameters for the adsorption of vanadate (adsorbate) onto iron-containing adsorbents from the literature. Units were converted for direct comparison of data.

Study	Adsorbent	Loading (mg g^{-1})	pH	Matrix	Freundlich	Langmuir
Gonzalez-Rodriguez and Fernandez-Marcos, 2021	Volcanic soil	0 – 2	5.6 – 6.3	0.02 mol L^{-1} $NaNO_3$	K_F = 4.95 – 5.50 m = 0.45 – 0.46	—
Kong et al., 2020	Nanoscale Fe^0 on layered double hydroxide	0 – 100	3.0	Groundwater	K_F = 37.8 n = 4.73	q_{max} = 87.0 K_L = 0.50
Naeem et al., 2007	Metal (hydr)oxides	0 – 180	6.9 – 7.2	0.01 mol L^{-1} $NaClO_4$	K_F = 9.20 – 42.8 n = 2.74–4.88	q_{max} = 25.1 – 111 K_L = 0.16 – 0.59*
Prathap and Namasivayam, 2010	Fe(III)/Cr(III) hydroxide	1 – 5	6.5 – 8.7	Distilled water	K_F = 0.58 – 4.56 n = 1.63 – 2.40	q_{max} = 4.93 – 11.4 K_L = 0.10 – 0.82
This study	**Carbonate green rust**	**0 – 6**	**7.5 – 8.5**	**Seawater (0.7 mol L^{-1})**	**K_F = 10.7 – 97.4 n = 1.01 – 1.46**	**q_{max} = 4.45 – 62.8 K_L = 1.71 – 9.81**
Vessey et al., 2020	Ferrihydrite and Hematite	0 – high	3 – 6	0.05 mol L^{-1} NaCl	—	K_L = 0.10 – 1.83
Zhu et al., 2020	Goethite and Birnessite	5 – 50	2 – 8	0.01 mol L^{-1} $NaNO_3$	K_F = 3.87 – 4.50 n = 4.35 – 5.56	q_{max} = 7.64 – 9.11 K_L = 0.52 – 1.52

Stumm, 1989). In contrast, vanadyl is mostly present as a cation ($V^{IV}O^{2+}$ and $V^{IV}OOH^{+}$) in aqueous systems and, therefore, adsorption onto green rust is generally favored for pH greater than 8.35 (Wehrli and Stumm, 1988), which may also explain the observed pH trends if most V^{V} was reduced to V^{IV} before adsorption.

4.4. Reductive sorption of V by green rust

We observed the reductive sorption of V by GR_{CO3} in seawater with an average solid-phase V oxidation state in between +5.0 to +4.0 for the pH range of seawater. Generally, V oxidation states decreased (XANES: +4.7 to +4.3) with decreasing pH (8.5 to 7.5). This trend could be explained by the increased concentration of aqueous Fe^{II} in solution at lower pH due to dissolution of GR_{CO3}, which could drive reduction of aqueous V (Frierdich and Catalano, 2012a, b). Generally, it should be noted that an average V valence state somewhere between +4.0 and +5.0 can be indicative of a mix of V^{V} and V^{IV}, but V^{III} may also be present (O'Loughlin et al., 2021). Here, with the additional analysis of EXAFS, a mix of mostly V^{V} and V^{IV} seemed to best fit the data. However, fitting models to vanadium EXAFS is a challenging task due to the complex coordination chemistry of vanadium species (e.g., Peacock and Sherman, 2004). Additionally, the data resolution for V *K*-edge data is of particular importance due to the overlapping of multiple V–O paths at low R (i.e., oxygen ligands anywhere between 1.6 Å and 2.2 Å). We have calculated the resolution of our data in R space (Rayleigh resolution criterion, see Equation S3) and found that ΔR was in between 0.14 Å and 0.19 Å, depending on the fitting range in k space (note that the fitting range in k space was always chosen as the maximum possible for the individual data set). Consequently, with the rather large discrepancy in resolution, the meaning of atomic distances and their errors must be put into perspective, and it should be acknowledged that slight differences in atomic distance (which may be required to distinguish vanadium species) may not be unequivocally distinguished by EXAFS modeling.

We provide evidence for the potential presence of both monodentate (V⋯Fe ~3.8 Å) and bidentate corner-sharing (V⋯Fe ~3.3 Å) V adsorption complexes, respectively. Density functional theory (DFT) calculations show that an increase in solution pH can generally be interpreted as a decrease in OH^{-} vacancies of GR_{CO3}, and therefore, bidentate sorption may be more likely at a lower pH and monodentate sorption at a higher pH. Prior studies on vanadate sorption have shown that a combination of both (monodentate and bidentate), and a transition to bidentate sorption complexes over time are energetically favored (Peacock and Sherman, 2004). The Hamilton test (Table S9) showed that these iron backscatters derived from the Fourier-transform carry a high statistical uncertainty, which can also be seen in the sinusoidal character of spectra and a lack in predominant features at higher R (Fig. 4). Previous groups have reported Fe backscatters for V EXAFS with a similar lack of predominant features and similar noise at higher k (e.g., Abernathy et al., 2022; Larsson et al., 2017a; Vessey and Lindsay, 2020). Here, we have included estimates of V–Fe paths, but acknowledge that these have a degree of uncertainty with them. Rather than suggesting a single possible coordination sphere, we found that a set of different possible coordinations can be fitted to the data – a common limitation of EXAFS (Cramer et al., 1978). We report the most coherent fit in the main text here, which we found to be a combination of potentially outer-sphere complexation, and a mixture of inner-sphere monodentate and bidentate corner-sharing complexes of V with green rust.

4.5. Oxidation of V-bearing green rust

We observed the complete oxidation of GR_{CO3} to lepidocrocite (LP) within 24 h in ambient air. The oxidation product(s) of carbonate green rust generally depend on factors such as impurities, reaction matrix (i.e., presence of anions/carbonate), temperature, pH, redox condition, and rate of oxygen input (Singh et al., 2010; Wang et al., 2013). When GR_{CO3} oxidizes in solution, a range of Fe^{III} (oxyhydr)oxides may form, including lepidocrocite [γ-FeO(OH)], goethite [α-FeO(OH)], a mix of both, or less commonly, ferrihydrite [$Fe_{10}O_{14}(OH)_2$] (Bernal et al., 1959; Randall et al., 2001; Legrand et al., 2004; Michel et al., 2007).

Oxidation of V-bearing GR_{CO3} to V-bearing LP resulted in the further reduction of V^{V} and incorporation of V^{IV}. Although it seems counterintuitive that the oxidation of GR would lead to the reduction of V, the oxidation of surface/structural Fe^{II} from GR_{CO3} yields a higher reduction potential than dissolved Fe^{II} (White and Peterson, 1996), which may lead to lower V oxidation states. Additionally, a significant pH decrease (down to as low as pH 5) was observed during the formation of the (oxyhydr)oxide mineral LP as OH^{-} was removed from solution. Vanadium reduction is generally favored in acidic solutions (Baes and Mesmer, 1976), demonstrated by the predominance of reduced V species under these conditions at equilibrium (Fig. S4). We hypothesize that the lower V oxidation states associated with LP may originate from a combination of both, the oxidation of surface/structural Fe^{II} (increase of free e^{-} to reduce V) as well as a significant decrease in solution pH.

The incorporation of V in Fe-bearing minerals has previously been reported: Sequestration of V has been shown in the case of synthetic goethite (Schwertmann and Pfab, 1994, 1996; Kaur et al., 2009), where V^{III} substituted for Fe^{III} due to their nearly identical atomic radii. Structural substitution of Fe with V^{IV} and V^{V} in goethite was also reported, with decreasing stability for increasing V oxidation state and temperature (Kaur et al., 2009). Aqueous Fe^{II} has been shown to mediate the release and structural incorporation of redox-sensitive trace metals into iron oxide phases (Frierdich and Catalano, 2012b, a). Further, Wehrli and Stumm (1989) calculated, based on adsorption data, that adsorption and subsequent incorporation of vanadyl (V^{IV}) may be an important mechanism for long-term sequestration of reduced V in sediments. A recent study confirmed this (Vessey and Lindsay, 2020) providing evidence for the incorporation of V^{IV}, and potentially V^{III}, in mackinawite ($Fe^{II}S$). In general, trivalent and bivalent iron in crystal structures of iron (oxyhydr)oxides can be replaced by metals of similar radii (Goldschmidt, 1937). Trivalent V has an ionic radius of ~0.640 Å, very similar to the ionic radius of trivalent Fe (~0.645 Å) (Shannon, 1976), while V^{IV} and V^{V} exhibit smaller ionic radii (~0.580 and ~0.355 Å). When occupying Fe-vacancies, differences in ionic size and in charge can cause crystal distortions (Singh et al., 2010).

We observed only minor (< 0.5%) release of V to solution during oxidation and a gradual decrease, with some local variations, in dissolved Fe. After 4 to 8 h of exposure to air, most of the residual Fe in solution (< 1 μM) was consumed by the oxidation reaction. These findings suggest that dissolution–coprecipitation of V and Fe and/or surface-catalyzed $Fe^{II}_{(aq)}$ oxidation and ion exchange could be possible mechanisms leading to the incorporation of reduced V in LP during the oxidation of V-bearing GR_{CO3}.

4.6. Vanadium and green rust interactions in the modern environment

While V can be utilized as a unique paleo-proxy for understanding early Earth systems, it also poses a threat to the modern environment as a toxic contaminant associated with anthropogenic activity (Hope, 2008; Schlesinger et al., 2017; Watt et al., 2018). Specifically, V^{V} and V^{IV} are considered harmful due to their toxicity and mobility in the environment (Crans et al., 1998; Larsson et al., 2015). In the context of V being an anthropogenic contaminant in modern terrestrial and aquatic environments, two studies have recently been published on the reduction and adsorption of V^{V} by GR (Table 5). O'Loughlin et al. (2021) provided evidence for a time-dependent reducing effect of both synthetic and biogenic sulfate GR ($SynGR_{SO4}$; $BioGR_{SO4}$), showing that after 4 months ($SynGR_{SO4}$) and after 20 months ($BioGR_{SO4}$), all adsorbed V^{V} (1000 μM) was fully reduced to V^{III} in pH 7.0 MOPS-buffered (0.05 M) suspension — based on XANES PEP analysis. Similarly, Vessey and Lindsay (2020) observed the formation of secondary chloride GR (GR_{Cl}) while assessing the interactions of $Fe^{II}_{(aq)}$ and vanadate (100 μM) in pH 7.0 [MOPS-buffered (0.005 M) NaCl (0.05 M)] solution. In contrast, our

Table 5
Comparison of context, form of green rust, study condition, vanadate concentration, study duration and V *K*-edge results of recent studies on vanadate (V^{V}) adsorption onto green rust.

Type of green rust (GR)	Study condition	Vanadate concentration	Study period	V *K*-edge XAS	Reference
Amorphous carbonate GR	pH 7.5 – 8.5; Synthetic seawater (salinity = 35‰)	20 μM (≙ 1 mg L^{-1})	Short term ('0' – 24 h)	XANES: **+4.3 – 4.7** EXAFS: monodentate and bidentate corner-sharing	This study
Biogenic sulfate GR	pH 7.0; MOPS (0.05 M)	1000 μM (≙ 50 mg L^{-1})	Short and long term (2 days to 20 months)	XANES: +**4.0** (2 days) and +**3.0** (> 4 months)	O'Loughlin et al., 2021
Secondary chloride GR	pH 7.0; NaCl (0.05 M) and MOPS (0.005 M)	100 μM (≙ 5 mg L^{-1})	Short term ('0' – 48 h)	XANES: +**4.31** (48 h) EXAFS:bidentate corner-sharing	Vessey and Lindsay, 2020

study was conducted at much higher ionic strength (~0.7 M) with lower total V concentration (20 μM, Wanty and Goldhaber, 1992), and using freshly precipitated carbonate GR to simulate authigenic GR formation in the seawater column (Zegeye et al., 2012). Overall, the solid-phase oxidation states of adsorbed V onto GR (short-term) reported by O'Loughlin et al. (2021) and Vessey and Lindsay (2020) compare well to our findings, with all observed V valence states being in between +4.0 and +5.0. Reduction of V^{V} to V^{III} by biogenic GR_{SO4} was reported by O'Loughlin et al. (2021). In light of these findings, the question arises whether vanadate would further reduce to V^{III} over longer time periods when adsorbed to amorphous GR surfaces in seawater. As the geochemistry of amorphous minerals can vary greatly to that of their more crystalline forms (e.g., following freeze drying; Rogers, 1917), investigating the sorption of V by amorphous/freshly precipitated phases may provide more environmentally-relevant data. With only a handful of studies addressing the geochemical relationship of V and mixed-valence iron phases, much remains to be studied, especially regarding V substitution in iron and sulfide minerals present in reducing marine conditions.

4.7. Implications and perspectives for modern and ancient marine settings

The results presented here have implications for the interpretation of solid-phase V speciation and enrichment in reducing marine environments, including ancient and modern oxygen-restricted/OMZ-type marine settings. In these environments, such as the Peruvian Margin, oxic waters commonly over- and underlie anoxic zones (Borchers et al., 2005; Scholz et al., 2011; Scholz, 2018), and green rust (in form of the oxidation product feroxyhyte) and lepidocrocite have both been reported here (Heller et al., 2017). Our study demonstrated that green rust (i.e., GR_{CO3}) may represent an effective sink for V in reducing environments of modern and ancient marine systems. Structural incorporation of V^{IV} into LP under these conditions, and its resistance to oxidation, may serve as an efficient vector aiding in the long-term enrichment of V in marine sediments. However, within the scope of this study we only investigated the short-term (up to 24 h) sorption/oxidation of V; GR/LP stabilities of adsorbed and incorporated V beyond this timeframe remain uncertain and require further attention in future works. Based on the findings of O'Loughlin et al. (2021), it can be speculated that with time all V^{V}/V^{IV} adsorbed onto GR_{CO3} will eventually be reduced to V^{III} under anoxic conditions. It is relevant to verify if this is the case under natural marine conditions and how stable V^{III} associated with GR_{CO3} is during fluctuating oxygen conditions and over extended periods of time (i.e., months to years). It is also critical to consider other transformation pathways for GR_{CO3} and similar V-loaded mineral phases in these environments, including reduction, oxidation, and sulfidation: which lead to mineral transformation reactions that influence the cycling of V in marine environments. While single-sorbent studies are essential for understanding basic geochemical interactions, natural sediment systems are much more complex and usually contain a wide range of iron (oxyhydr)oxides as well as other minerals and metals with the potential for competitive sorption. Therefore, processes observed in single-sorbent studies, such as this one, should be further investigated in more complex, natural sedimentary systems.

5. Conclusion

We found vanadate to be rapidly, and efficiently, reduced and removed from solution by GR_{CO3} across the pH range typical of seawater. Following partial reduction and adsorption by GR, oxidation of V-bearing GR_{CO3} to LP did not result in any significant release of V into solution; rather, solid-phase V was further reduced to V^{IV} and incorporated into the structure of the newly formed LP. Incorporation of V^{IV} prevented reoxidation to V^{V} over the 24-hour timescale of the experiment. These results support the important role green rusts and secondary Fe^{III} (oxyhydr)oxides (i.e., LP) may have in the transport of V from the water column to the sediment. Overall, to gain a better understanding of authigenic V enrichment in anoxic sediments, and for the accurate interpretation of V in the sedimentary rock record, an improved understanding of the cycling and stability of V in marine oxygen-restricted environments and its relationship with other (iron) minerals during early diagenesis is required.

Declaration of Competing Interest

The authors declare that they have no known competing financial interests or personal relationships that could have appeared to influence the work reported in this paper.

Acknowledgements

Sample analysis for this research was undertaken at the XAS beamline of the Australian Synchrotron, part of ANSTO. Further, this study was supported by an ARC Discovery Project grant (DP180100531; to WB, EL, DC) to investigate the geochemistry of vanadium in modern and ancient sediments, as well as by a Griffith University PhD Scholarship and an AINSE Ltd. Postgraduate Research Award (PGRA) to FH. In addition, DC would like to acknowledge support from the Villum Foundation, Denmark (Grant No. 16518). We would like to thank Dr. Nick Ward and Dr. Niloofar Karimian who kindly performed the XRD analysis for our oxygen-sensitive mineral samples and Dr. Edward D. Burton for his insight on the geochemistry and definition of green rust minerals. Lastly, we would like to thank the reviewers for their in-depth and knowledgeable revisions, which helped to substantially improve the quality of the manuscript.

Appendix A. Supplementary material

The supplementary data includes a supplementary material file with additional research data (tables and figures referred to in the main text) as well as a summary Excel file of the raw research data "V-GR Research Data". Further research data will be made available upon request. Supplementary data to this article can be found online at https://doi.org/10.1016/j.gca.2023.07.020.

References

Abernathy, M.J., Schaefer, M.V., Vessey, C.J., Liu, H., Ying, S.C., 2021. Oxidation of V (IV) by birnessite: kinetics and surface complexation. Environ. Sci. Tech. 55, 11703–11712.
Abernathy, M.J., Schaefer, M.V., Ramirez, R., Garniwan, A., Lee, I., Zaera, F., Polizzotto, M.L., Ying, S.C., 2022. Vanadate retention by iron and manganese oxides. ACS Earth Sp. Chem. 6, 2041–2052.
Algeo, T.J., Maynard, J.B., 2004. Trace-element behavior and redox facies in core shales of Upper Pennsylvanian Kansas-type cyclothems. Chem. Geol. 206, 289–318.
Baes, C.F., Mesmer, R.E., 1976. The Hydrolysis of Cations, first ed. John Wiley & Sons, New York.
Balan, E., De Villiers, J.P.R., Eeckhout, S.G., Glatzel, P., Toplis, M.J., Fritsch, E., Allard, T., Galoisy, L., Calas, G., 2006. The oxidation state of vanadium in titanomagnetite from layered basic intrusions. American Mineralogist 91, 953–956.
Bennett, W.W., Canfield, D.E., 2020. Redox-sensitive trace metals as paleoredox proxies: A review and analysis of data from modern sediments. Earth-Science Rev. 204, 103175.
Bennett, W.W., Lombi, E., Burton, E.D., Johnston, S.G., Kappen, P., Howard, D.L., Canfield, D.E., 2018. Synchrotron X-ray spectroscopy for investigating vanadium speciation in marine sediment: limitations and opportunities. J. Anal. At. Spectrom 33, 1689–1699.
Benzi, F., Giuli, G., Della, L.S., Paris, E., 2016. Vanadium K-edge XANES in vanadium-bearing model compounds: A full multiple scattering study. J. Synchrotron Radiat. 23, 947–952.
Bernal, J.D., Dasgupta, D.R., Mackay, A.L., 1959. The oxides and hydroxides of iron and their structural inter-relationships. Clay Miner. Bull. 4, 15–30.
Bian, L., Chappaz, A., Schovsbo, N.H., Sanei, H., 2022. A new vanadium species in black shales: Updated burial pathways and implications. Geochim. Cosmochim. Acta 338, 1–10.
Bocher, F., Géhin, A., Ruby, C., Ghanbaja, J., Abdelmoula, M., Génin, J.-M.-R., 2004. Coprecipitation of Fe (II–III) hydroxycarbonate green rust stabilised by phosphate adsorption. Solid State Sci. 6, 117–124.
Bond, D.L., Fendorf, S., 2003. Kinetics and structural constraints of chromate reduction by green rusts. Environ. Sci. Tech. 37, 2750–2757.
Borchers, S.L., Schnetger, B., Böning, P., Brumsack, H.-J., 2005. Geochemical signatures of the Namibian diatom belt: Perennial upwelling and intermittent anoxia. Geochem. Geophys. Geosyst. 6, Q06006.
Brinza, L., Benning, L.G., Statham, P.J., 2008. Adsorption studies of Mo and V onto ferrihydrite. Mineral. Mag. 72, 385–388.
Brinza, L., Vu, H.P., Neamtu, M., Benning, L.G., 2019. Experimental and simulation results of the adsorption of Mo and V onto ferrihydrite. Sci. Rep. 9, 1–12.
Brumsack, H.J., 2006. The trace metal content of recent organic carbon-rich sediments: Implications for Cretaceous black shale formation. Palaeogeogr. Palaeoclimatol. Palaeoecol. 232, 344–361.
Calvin, S., 2013. XAFS for Everyone, first ed. CRC Press, Boca Raton.
Canfield, D.E., Zhang, S., Wang, H., Wang, X., Zhao, W., Su, J., Bjerrum, C.J., 2018. A Mesoproterozoic iron formation. PNAS 115, 3895–3904.
Chaurand, P., Rose, J., Briois, V., Salome, M., Proux, O., Nassif, V., Olivi, L., Susini, J., Hazemann, J.L., Bottero, J.Y., 2007. New methodological approach for the vanadium K-edge X-ray absorption near-edge structure interpretation: application to the speciation of vanadium in oxide phases from steel slag. J. Phys. Chem. B 111, 5101–5110.
Chen, G., Liu, H., 2017. Understanding the reduction kinetics of aqueous vanadium (V) and transformation products using rotating ring-disk electrodes. Environ. Sci. Tech. 51, 11643–11651.
Collier, R.W., 1984. Particulate and dissolved vanadium in the North Pacific Ocean. Nature 309, 441–444.
Cooper, M.A., Hawthorne, F.C., Grice, J.D., 2003. Anorthominasragrite, $V^{4+}O(SO_4)(H_2O)_5$, A new mineral species from Temple Mountain, Emery County, Utah, U.S.A.: description, crystal structure and hydrogen bonding. Can. Mineral. 41, 959–979.
Cramer, S.P., Hodgson, K.O., Stiefel, E.I., Newton, W.E., 1978. A systematic X-ray absorption study of molybdenum complexes. The Accuracy of Structural information from extended X-ray absorption fine structure. J. Am. Chem. Soc. 2748–2761.
Crans, D.C., Amin, S.S., Keramidas, A.D., 1998. Chemistry of relevance to vanadium in the environment. In: Nriagu, J.O. (Ed.), Vanadium in the Environment. Part 1: Chemistry and Biochemistry. John Wiley & Sons, New York, pp. 73–95.
Crans, D.C., Zhang, B., Gaidamauskas, E., Keramidas, A.D., Willsky, G.R., Roberts, C.R., 2010. Is vanadate reduced by thiols under biological conditions? Changing the redox potential of V (V) / V (IV) by complexation in aqueous solution. Inorg. Chem. 49, 4245–4256.
Cruywagen, J.J., 1999. Protonation, oligomerization, and condensation reactions of vanadate (V), molybdate (VI), and tungstate (VI). Adv. Inorg. Chem. 49, 127–182.
Drissi, S.H., Refait, P., Abdelmoula, M., Génin, J.M.R., 1995. The preparation and thermodynamic properties of Fe (II) – Fe (III) hydroxide-carbonate (green rust 1); Pourbaix diagram of iron in carbonate-containing aqueous media. Corros. Sci. 37, 2025–2041.
Duchesne, M.A., Nakano, J., Hu, Y., MacLennan, A., Hughes, R.W., Bennett, J., Nakano, A., 2016. Vanadium oxidation state determination by X-ray absorption spectroscopy. In: Reddy, R.G., Chaubal, P., Pistorius, P.C., Pal, U. (Eds.), Advances in Molten Slags, Fluxes, and Salts: Proceedings of The 10th International Conference on Molten Slags, Fluxes and Salts (MOLTEN16), pp. 1405–1412.
Etique, M., Jorand, F.P.A., Zegeye, A., Grégoire, B., Despas, C., Ruby, C., 2014. Abiotic process for Fe (II) oxidation and green rust mineralization driven by a heterotrophic nitrate reducing bacteria (Klebsiella mobilis). Environ. Sci. Tech. 48, 3742–3751.
Ewing, F.J., 1935. The crystal structure of lepidocrocite. J. Chem. Phys. 3, 420–424.
Freundlich, H., 1906. Über die Adsorption in Lösungen. Zeitschrift für Phys. Chemie 57, 385–470.
Frierdich, A.J., Catalano, J.G., 2012a. Controls on Fe(II)-activated trace element release from goethite and hematite. Environ. Sci. Tech. 46, 1519–1526.
Frierdich, A.J., Catalano, J.G., 2012b. Fe(II)-mediated reduction and repartitioning of structurally incorporated Cu Co, and Mn in iron oxides. Environ. Sci. Tech. 46, 11070–11077.
Gehring, A.U., Fry, I.V., Luster, J., Sposito, G., 1994. Vanadium in sepiolite: A redox-indicator for an ancient closed brine system in the Madrid Basin, central Spain. Geochim. Cosmochim. Acta 58, 3345–3351.
Génin, J.-M.R., Christy, A., Kuzmann, E., Mills, S., Ruby, C., 2014. Structure and occurrences of green rust related new minerals of the fougerite group, trebeurdenite and mössbauerite, belonging to the hydrotalcite supergroup; how Mössbauer spectroscopy helps XRD. Hyperfine Interact. 226, 459–482.
Goldschmidt, V.M., 1937. The Principles of Distribution of Chemical Elements in Minerals and Rocks. pp. 655–673.
Gonzalez-Rodriguez, S., Fernandez-Marcos, M.L., 2021. Sorption and desorption of vanadate, arsenate and chromate by two volcanic soils of Equatorial Africa. Soil Syst. 5, 22.
Guilbaud, R., White, M.L., Poulton, S.W., 2013. Surface charge and growth of sulphate and carbonate green rust in aqueous media. Geochim. Cosmochim. Acta 108, 141–153.
Gustafsson, J.P., 2019. Vanadium geochemistry in the biogeosphere –speciation, solid-solution interactions, and ecotoxicity. Appl. Geochem. 102, 1–25.
Halevy, I., Alesker, M., Schuster, E.M., Popovitz-Biro, R., Feldman, Y., 2017. A key role for green rust in the Precambrian oceans and the genesis of iron formations. Nat. Geosci. 10, 135.
Han, T., Fan, H., Wen, H., 2018. Dwindling vanadium in seawater during the early Cambrian, South China. Chem. Geol. 492, 20–29.
Hansen, H.C.B., Koch, C.B., Nancke-Krogh, H., Borggaard, O.K., Sørensen, J., 1996. Abiotic nitrate reduction to ammonium: Key role of green rust. Environ. Sci. Tech. 30, 2053–2056.
Haskel, D., Islam, Z., Lang, J., Kmety, C., Srajer, G., Pokhodnya, K.I., Epstein, A.J., Miller, J.S., 2004. Local structural order in the disordered vanadium tetracyanoethylene room-temperature molecule-based magnet. Phys. Rev. B -Condens. Matter Mater. Phys. 70, 1–9.
Heller, M.I., Lam, P.J., Moffett, J.W., Till, C.P., Lee, J., Toner, B.M., Marcus, M.A., 2017. Accumulation of Fe oxyhydroxides in the Peruvian oxygen deficient zone implies non-oxygen dependent Fe oxidation. Geochim. Cosmochim. Acta 211, 174–193.
Ho, P., Lee, J.M., Heller, M.I., Lam, P.J., Shiller, A.M., 2018. The distribution of dissolved and particulate Mo and V along the U.S. GEOTRACES East Pacific Zonal Transect (GP16): The roles of oxides and biogenic particles in their distributions in the oxygen deficient zone and the hydrothermal plume. Mar. Chem. 201, 242–255.
Hope, B.K., 2008. A dynamic model for the global cycling of anthropogenic vanadium. Global Biogeochem. Cycles 22, 1–16.
Huang, J.H., Huang, F., Evans, L., Glasauer, S., 2015. Vanadium: Global (bio) geochemistry. Chem. Geol. 417, 68–89.
Jeandel, C., Caisso, M., Minster, J.F., 1987. Vanadium behaviour in the global ocean and in the Mediterranean sea. Mar. Chem. 21, 51–74.
Jönsson, J., Sherman, D.M., 2008. Sorption of As (III) and As (V) to siderite, green rust (fougerite) and magnetite: Implications for arsenic release in anoxic groundwaters. Chem. Geol. 255, 173–181.
Karimian, N., Johnston, S.G., Burton, E.D., 2017. Antimony and arsenic behavior during Fe (II) -induced transformation of jarosite. Environ. Sci. Tech. 51, 4259–4268.
Kaur, N., Singh, B., Kennedy, B.J., Gräfe, M., 2009. The preparation and characterization of vanadium-substituted goethite: The importance of temperature. Geochim. Cosmochim. Acta 73, 582–593.
Koeksoy, E., Halama, M., Konhauser, K.O., Kappler, A., 2016. Using modern ferruginous habitats to interpret Precambrian banded iron formation deposition. Int. J. Astrobiol. 15, 205–217.
Koeksoy, E., Sundman, A., Byrne, J.M., Lohmayer, R., Planer-Friedrich, B., Halevy, I., Konhauser, K.O., Kappler, A., 2019. Formation of green rust and elemental sulfur in an analogue for oxygenated ferro-euxinic transition zones of Precambrian oceans. Geology 47, 211–214.
Kong, X., Chen, J., Tang, Y., Lv, Y., Chen, T., Wang, H., 2020. Enhanced removal of vanadium (V) from groundwater by layered double hydroxide-supported nanoscale zerovalent iron. J. Hazard. Mater. 392, 122392.
Kostka, J.E., Luther III, G.W., 1994. Partitioning and speciation of solid phase iron in saltmarsh sediments. Geochim. Cosmochim. Acta 58, 1701–1710.
Kraft, S., Stümpel, J., Becker, P., Kuetgens, U., 1996. High resolution x-ray absorption spectroscopy with absolute energy calibration for the determination of absorption edge energies. Rev. Sci. Instrum. 67, 681–687.
Krakowiak, J., Lundberg, D., Persson, I., 2012. A coordination chemistry study of hydrated and solvated cationic vanadium ions in oxidation states +III, +IV, and +V in solution and solid state. Inorg. Chem. 51, 9598–9609.
Krauskopf, K.B., 1956. Factors controlling the concentrations of thirteen rare metals in sea-water. Geochim. Cosmochim. Acta 9, 1–32.
Langmuir, I., 1916. The constitution and fundamental properties of solids and liquids. J. Am. Chem. Soc. 38, 2221–2295.

Langmuir, I., 1918. The adsorption of gases on plane surfaces of glass, mica and platinum. J. Am. Chem. Soc. 40, 1361–1403.
Larsson, M.A., Baken, S., Smolders, E., Cubadda, F., Gustafsson, J.P., 2015. Vanadium bioavailability in soils amended with blast furnace slag. J. Hazard. Mater. 296, 158–165.
Larsson, M.A., Hadialhejazi, G., Gustafsson, J.P., 2017a. Vanadium sorption by mineral soils: Development of a predictive model. Chemosphere 168, 925–932.
Larsson, M.A., Persson, I., Sjöstedt, C., Gustafsson, J.P., 2017b. Vanadate complexation to ferrihydrite: X-ray absorption spectroscopy and CD-MUSIC modelling. Environ. Chem. 14, 141–150.
Legrand, L., Mazerolles, L., Chausse, A., 2004. The oxidation of carbonate green rust into ferric phases: solid-state reaction or transformation via solution. Geochim. Cosmochim. Acta 68, 3497–3507.
Levina, A., Mcleod, A.I., Lay, P.A., 2014. Vanadium speciation by XANES spectroscopy: A three-dimensional approach. Chem. - A Eur. J. 20, 12056–12060.
Lewan, M.D., 1984. Factors controlling the proportionality of vanadium to nickel in crude oils. Geochim. Cosmochim. Acta 48, 2231–2238.
Michel, M.F., Ehm, L., Antao, S.M., Lee, P.L., Chupas, P.J., Liu, G., Strongin, D.R., Schoonen, M.A.A., Phillips, B.L., Parise, J.B., 2007. The structure of ferrihydrite, a nanocrystalline material. Science 80-.). 316, 1726–1729.
Mills, S.J., Christy, A.G., Génin, J.-M.-R., Kameda, T., Colombo, F., 2012. Nomenclature of the hydrotalcite supergroup: natural layered double hydroxides. Mineral. Mag. 76, 1289–1336.
Mitsunobu, S., Takahashi, Y., Sakai, Y., 2008. Abiotic reduction of antimony (V) by green rust ($Fe_4(II)Fe_2(III)(OH)_{12}SO_4 \cdot 3H_2O$). Chemosphere 70, 942–947.
Morford, J.L., Emerson, S.R., Breckel, E.J., Kim, S.H., 2005. Diagenesis of oxyanions (V, U, Re, and Mo) in pore waters and sediments from a continental margin. Geochim. Cosmochim. Acta 69, 5021–5032.
Myneni, S.C.B., Tokunaga, T.K., Brown Jr., G.E., 1997. Abiotic selenium redox transformations in the presence of Fe (II, III) oxides. Science (80-.) 278, 1106–1109.
Naeem, A., Westerhoff, P., Mustafa, S., 2007. Vanadium removal by metal (hydr) oxide adsorbents. Water Res. 41, 1596–1602.
O'Loughlin, E.J., Kelly, S.D., Cook, R.E., Csencsits, R., Kemner, K.M., 2003. Reduction of uranium (VI) by mixed iron (II)/iron (III) hydroxide (green rust): Formation of UO_2 nanoparticles. Environ. Sci. Tech. 37, 721–727.
O'Loughlin, E.J., Boyanov, M.I., Kemner, K.M., 2021. Reduction of vanadium (V) by iron (II) - bearing minerals. Minerals 11, 316.
Ona-Nguema, G., Abdelmoula, M., Jorand, F., Benali, O., Géhin, A., Block, J.C., Génin, J. M.R., 2002. Iron (II, III) hydroxycarbonate green rust formation and stabilization from lepidocrocite bioreduction. Environ. Sci. Tech. 36, 16–20.
Peacock, C.L., Sherman, D.M., 2004. Vanadium (V) adsorption onto goethite (α-FeOOH) at pH 1.5 to 12: a surface complexation model based on ab initio molecular geometries and EXAFS spectroscopy. Geochim. Cosmochim. Acta 68, 1723–1733.
Perez, J.P.H., Freeman, H.M., Schuessler, J.A., Benning, L.G., 2019. The interfacial reactivity of arsenic species with green rust sulfate (GR SO4). Sci. Total Environ. 648, 1161–1170.
Prathap, K., Namasivayam, C., 2010. Adsorption of vanadate (V) on Fe (III) / Cr (III) hydroxide waste. Environ. Chem. Lett. 8, 363–371.
Randall, S.R., Sherman, D.M., Ragnarsdottir, K.V., 2001. Sorption of As (V) on green rust ($Fe_4(II)Fe_2(III)(OH)_{12}SO_4 \cdot 3H_2O$) and lepidocrocite (y-FeOOH): Surface complexes from EXAFS spectroscopy. Geochim. Cosmochim. Acta 65, 1015–1023.
Ravel, B., Newville, M., 2005. Athena, Arthemis, Hephaestus: Data analysis for X-ray absorption spectroscopy using IFEFFIT. J. Synchrotron Radiat. 12, 537–541.
Rogers, A.F., 1917. A review of the amorphous minerals. J. Geol. 25, 515–541.
Ruby, C., Abdelmoula, M., Khare, V., Ona-Nguema, G., Morin, G., Genin, J.-M.R., 2010. Oxidation modes and thermodynamics of Fe II – III oxyhydroxycarbonate green rust : Dissolution – precipitation versus in situ deprotonation. Geochim. Cosmochim. Acta 74, 953–966.
Russell, M.J., Ponce, A., 2020. Six 'must-have' minerals for life's emergence: olivine, pyrrhotite, bridgmanite, serpentine, fougerite and mackinawite. Life 10, 291.
Sadiq, M., 1988. Thermodynamic solubility relationships of inorganic vanadium in the marine environment. Mar. Chem. 23, 87–96.
Scatchard, G., 1949. The attraction of proteins for small molecules and ions. Ann. N. Y. Acad. Sci. 51, 660–672.
Schlesinger, W.H., Klein, E.M., Vengosh, A., 2017. Global biogeochemical cycle of vanadium. PNAS 114, E11092–E11100.
Scholz, F., 2018. Identifying oxygen minimum zone-type biogeochemical cycling in Earth history using inorganic geochemical proxies. Earth-Science Rev. 184, 29–45.
Scholz, F., Hensen, C., Noffke, A., Rohde, A., Liebetrau, V., Wallmann, K., 2011. Early diagenesis of redox-sensitive trace metals in the Peru upwelling area – response to ENSO-related oxygen fluctuations in the water column. Geochim. Cosmochim. Acta 75, 7257–7276.
Schwertmann, U., Pfab, G., 1994. Structural vanadium in synthetic goethite. Geochim. Cosmochim. Acta 58, 4349–4352.
Schwertmann, U., Pfab, G., 1996. Structural vanadium and chromium in lateritic iron oxides: Genetic implications. Geochim. Cosmochim. Acta 60, 4279–4283.
Shaheen, S.M., Alessi, D.S., Tack, F.M.G., Ok, Y.S., Kim, K.H., Gustafsson, J.P., Sparks, D. L., Rinklebe, J., 2019. Redox chemistry of vanadium in soils and sediments: Interactions with colloidal materials, mobilization, speciation, and relevant environmental implications - A review. Adv. Colloid Interface Sci. 265, 1–13.
Shannon, R.D., 1976. Revised effective ionic radii and systematic studies of interatomie distances in halides and chaleogenides. Acta Crystall. Section A 32, 751–767.
Shieh, C.S., Duedall, I.W., 1988. Role of amorphous ferric oxyhydroxide in removal of anthropogenic vanadium from seawater. Mar. Chem. 25, 121–139.
Singh, B., Gräfe, M., Kaur, N., Liese, A., 2010. Applications of synchrotron-based X-ray diffraction and X-ray absorption spectroscopy to the understanding of poorly crystalline and metal-substituted Iron oxides. Dev. Soil Sci. 34, 199–254.
Taylor, M.J.C., Van Staden, J.F., 1994. Spectrophotometric determination of vanadium (IV) and vanadium (V) in each other's presence. Analyst 119, 1263–1276.
Trefry, J.H., Metz, S., 1989. Role of hydrothermal precipitates in the geochemical cycling of vanadium. Nature 342, 531–533.
Tribovillard, N., Algeo, T.J., Lyons, T., Riboulleau, A., 2006. Trace metals as paleoredox and paleoproductivity proxies: An update. Chem. Geol. 232, 12–32.
Trolard, F., Génin, J.M.R., Abdelmoula, M., Bourrié, G., Humbert, B., Herbillon, A., 1997. Identification of a green rust mineral in a reductomorphic soil by Mössbauer and Raman spectroscopies. Geochim. Cosmochim. Acta 61, 1107–1111.
Trolard, F., Bourrie, G., Abdelmoula, M., Refrait, P., Feder, F., 2007. Fougerite, a new mineral of the pyroaurite-iowaite group: description and crystal structure. Clays Clay Miner. 55, 323–334.
Vessey, C.J., Lindsay, M.B.J., 2020. Aqueous vanadate removal by iron (II) -bearing phases under anoxic conditions. Environ. Sci. Tech. 54, 4006–4015.
Vessey, C.J., Schmidt, M.P., Abdolahnezhad, M., Peak, D., Lindsay, M.B.J., 2020. Adsorption of (poly) vanadate onto ferrihydrite and hematite: an in situ ATR–FTIR Study. ACS Earth Sp. Chem. 4, 641–649.
Vine, J.D., Tourtelot, E.B., 1970. Geochemistry of black shale deposits - A summary report. Econ. Geol. 65, 253–272.
Wang, J., Guo, X., 2020. Adsorption isotherm models: Classification, physical meaning, application and solving method. Chemosphere 258, 127279.
Wang, X., Liu, F., Tan, W., Feng, X., Koopal, L.K., 2013. Transformation of hydroxycarbonate green rust into crystalline iron (hydr) oxides: Influences of reaction conditions and underlying mechanisms. Chem. Geol. 351, 57–65.
Wang, X., Li, L., Liu, J., Wu, Y., Gao, J., Cao, P., Zhang, Y., Shi, X., 2019. Early diagenesis of redox-sensitive trace metals in the northern Okinawa Trough. Acta Oceanol. Sin. 38, 14–25.
Wang, D., Sañudo Wilhelmy, S.A., 2008. Development of an analytical protocol for the determination of V (IV) and V (V) in seawater: Application to coastal environments. Mar. Chem. 112, 72–80.
Wang, D., Sañudo Wilhelmy, S.A., 2009. Vanadium speciation and cycling in coastal waters. Mar. Chem. 117, 52–58.
Wanty, R.B., Goldhaber, M.B., 1992. Thermodynamics and kinetics of reactions involving vanadium in natural systems: Accumulation of vanadium in sedimentary rocks. Geochim. Cosmochim. Acta 56, 1471–1483.
Watt, J.A.J., Burke, I.T., Edwards, R.A., Malcolm, H.M., Mayes, W.M., Olszewska, J.P., Pan, G., Graham, M.C., Heal, K.V., Rose, N.L., Turner, S.D., Spears, B.M., 2018. Vanadium: A Re-emerging environmental hazard. Environ. Sci. Technol. 52, 11973–11974.
Wehrli, B., Stumm, W., 1988. Oxygenation of vanadyl (IV). Effect of coordinated surface hydroxyl groups and OH^-. Langmuir 4, 753–758.
Wehrli, B., Stumm, W., 1989. Vanadyl in natural waters: Adsorption and hydrolysis promote oxygenation. Geochim. Cosmochim. Acta 53, 69–77.
Wen, B., Wang, Q., Lin, Y., Chernova, N.A., Karki, K., Chung, Y., Omenya, F., Sallis, S., Piper, L.F.J., Ong, S.P., Whittingham, M.S., 2016. Molybdenum substituted V \vanadyl phosphate ε - VOPO4 with enhanced two-electron transfer reversibility and kinetics for lithium-ion batteries. Chem. Mater. 28, 3159–3170.
White, A.F., Peterson, M.L., 1996. Reduction of aqueous transition metal species on the surfaces of Fe (II) -containing oxides. Geochim. Cosmochim. Acta 60, 3799–3814.
Williams, A.G.B., Scherer, M.M., 2001. Kinetics of Cr (VI) reduction by carbonate green rust. Environ. Sci. Tech. 35, 3488–3494.
Wisawapipat, W., Kretzschmar, R., 2017. Solid phase speciation and solubility of vanadium in highly weathered soils. Environ. Sci. Tech. 51, 8254–8262.
Wong, J., Lytle, F.W., Messmer, R.P., Maylotte, D.H., 1984. K-edge absorption spectra of selected vanadium compounds. Phys. Rev. B 30, 5596–5610.
Zegeye, A., Bonneville, S., Benning, L.G., Sturm, A., Fowle, D.A., Jones, C.A., Canfield, D. E., Ruby, C., MacLean, L.C., Nomosatryo, S., Crowe, S.A., Poulton, S.W., 2012. Green rust formation controls nutrient availability in a ferruginous water column. Geology 40, 599–602.
Zhang, S., Wang, X., Wang, H., Bjerrum, C.J., Hammarlund, E.U., Costa, M.M., Connelly, J.N., Zhang, B., Su, J., Canfield, D.E., 2016. Sufficient oxygen for animal respiration 1,400 million years ago. PNAS 113, 1731–1736.
Zhao, J., Xiong, S., Ai, J., Wu, J., Huang, L.Z., Yin, W., 2021. Stabilized green rusts for aqueous Cr (VI) removal: fast kinetics, high iron utilization rate and anti-acidification. Chemosphere 262, 127853.
Zhu, H., Xiao, X., Guo, Z., Peng, C., Wang, X., Yang, A., 2020. Characteristics and behaviour of vanadium (V) adsorption on goethite and birnessite. Environ. Earth Sci. 79, 1–10.